Journal of Alloys and Compounds 507 (2010) 370–375

Contents lists available at ScienceDirect

Journal of Alloys and Compounds

journal homepage: www.elsevier.com/locate/jallcom

Magnetic and magnetocaloric properties of the ternary Gd-based metallic glasses $Gd_{60}Mn_{30}X_{10}$, with X = Al, Ga, In

C. Mayer[a], B. Chevalier[a,*], S. Gorsse[a,b]

[a] CNRS, Université de Bordeaux, ICMCB, 87 avenue du Docteur Albert Schweitzer, 33608 Pessac Cedex, France
[b] IPB, ENSCPB, 16 avenue Pey-Berland, 33607 Pessac, France

ARTICLE INFO

Article history:
Received 24 June 2010
Received in revised form 23 July 2010
Accepted 28 July 2010
Available online 4 August 2010

Keywords:
Metallic glasses
Nanocomposites
X-ray powder diffraction
Magnetocaloric effect

ABSTRACT

Magnetocaloric effect and refrigeration capacity (RC) of $Gd_{60}Mn_{30}Ga_{10}$ and $Gd_{60}Mn_{30}In_{10}$ melt-spun nanocomposites are investigated. It is found that the nanocrystallites formed in the amorphous matrix are different between melt-spun $Gd_{60}Mn_{30}Ga_{10}$ and $Gd_{60}Mn_{30}In_{10}$ samples. $Gd_{60}Mn_{30}Ga_{10}$ ribbons exhibit multiple second-order transitions in accordance to their composite nature whereas $Gd_{60}Mn_{30}In_{10}$ ribbons display only one magnetic transition. The occurrence of several transitions increases the gap of temperature at half maximum value of the ΔS_M magnetic entropy, thus increasing the RC values of these materials. The use of Mn as transition metal induces Curie temperature values around 170–180 K and an antiferromagnetic coupling with Gd reducing the overall magnetization compared to that calculated considering the free Gd^{3+} ion.

1. Introduction

The magnetocaloric effect (MCE) consists in the temperature change of magnetic materials under the application of an external magnetic field. This MCE is the key effect upon which is based the highly promising and eco-friendly magnetic refrigeration technology [1]. Although it has already been used for refrigeration at very low temperatures with paramagnetic salts [2], magnetic refrigeration at room temperature is not yet a mature technology. The challenge is then to obtain materials exhibiting high magnetic refrigeration efficiency near room temperature under relatively low applied magnetic fields. A relevant parameter often used in the literature to characterize the refrigerant efficiency of a material is the refrigeration capacity (RC) defined as the area below the magnetic entropy change (ΔS_M) *versus T* curve, with the temperatures at half maximum of the peak as the integration limits [3]. Good materials for magnetic refrigeration should then present both a high magnetic entropy change ΔS_M and a broad ΔS_M peak.

Since a few years, the study of amorphous rare-earth based [4–15] materials and especially ternary Gd-based amorphous alloys [6–8,10,11,13–15] increased widely as those materials display interesting properties for magnetic refrigeration: they usually have a low electric resistivity that decreases eddy current losses, a tuneable ordering temperature, a high corrosion resistance and good mechanical properties [16].

Among all ternary Gd-M-X (M = transition metal and X = p-element) metallic glasses reported previously: (i) those containing Mn as M transition metal have higher Curie temperatures [7] and (ii) almost all of them have Al as p-element. Moreover, to guaranty a good glass forming ability, calculations based on a method described elsewhere [17,18], were conducted and indicated that $Gd_{60}Mn_{30}X_{10}$ composition had a great amorphization potential.

In a previous work, Gorsse et al. [7] have shown that the nanocomposite structure of melt-spun $Gd_{60}Mn_{30}Al_{10}$ could lead to the enlargement of the temperature range over which the transition happens, by the succession of several magnetic transitions (due to the coexistence of the amorphous matrix and gadolinium nanoprecipitates) occurring at different temperatures. To develop this nanocomposites approach, we have synthesized a series of $Gd_{60}Mn_{30}X_{10}$ (X = Al, Ga, In) metallic glasses in which Al was replaced by Ga or In to investigate the nature of the nanoprecipitates obtained by this change of X p-element. Furthermore, no ternary compounds containing more than 33.3 at.% of Gd are reported in the Gd–Mn–X, with X = Ga, In systems. We report here the structural, magnetic and magnetocaloric properties of these $Gd_{60}Mn_{30}X_{10}$ melt-spun materials.

2. Experimental

Alloys with the following compositions (at.%), $Gd_{60}Mn_{30}X_{10}$ with X = Al, Ga, In, were prepared by melting precisely weighted amounts of high purity elements Gd, Mn, Al and In (99.9%), and Ga (99.99%) in a levitation furnace. Melting was performed several times to ensure a good homogeneity, in a water-cooled copper crucible, under a purified argon atmosphere. The weight losses during the overall melting process were less than 0.1 wt.%. Metallic ribbons of these as-cast samples were obtained

* Corresponding author.
E-mail address: chevalie@icmcb-bordeaux.cnrs.fr (B. Chevalier).

0925-8388/$ – see front matter © 2010 Elsevier B.V. All rights reserved.
doi:10.1016/j.jallcom.2010.07.210

Table 1
Phases detected by XRD in as-cast and melt-spun samples.

Sample	As-cast state	Melt-spun state
$Gd_{60}Mn_{30}Al_{10}$	α-Gd, $GdMn_{1.6}Al_{0.4}$	Amorphous, α-Gd
$Gd_{60}Mn_{30}Ga_{10}$	α-Gd, Gd_5Ga_3, $GdMn_2$	Amorphous, α-Gd
$Gd_{60}Mn_{30}In_{10}$	Gd(In), Gd_2In, $GdMn_2$	Amorphous, Gd(In), Gd_2In

by single-roller melt-spinning technique with a copper wheel velocity between 25 and 30 m s^{-1} in a purified argon atmosphere.

Structural characterizations of both as-cast samples and melt-spun ribbons were performed with X-ray powder diffraction (XPD) using a Philips PW 1050 diffractometer with Cu Kα radiation and transmission electron microscopy (TEM) with a JEOL JEM 2000 FX apparatus.

DC magnetization measurements were realized using a superconducting quantum interface device magnetometer (SQUID) in the temperature range of 5–360 K and applied fields up to 4.6 T.

3. Results and discussion

X-ray powder diffraction (XPD) measurements, performed on the as-cast $Gd_{60}Mn_{30}X_{10}$ samples, reveal the presence of multiple phases in good agreement with their ternary Gd–Mn–X phase diagrams. For instance, the three compounds α-Gd [19], $GdMn_2$ [20] and Gd_5Ga_3 [21] are detected in as-cast $Gd_{60}Mn_{30}Ga_{10}$ sample (Fig. 1(a)).

As indicated in Table 1, as-cast samples contain $GdMn_2$ [22] when X = Ga, $GdMn_2$ doped by In atoms [23] when X = In, or a solid solution $GdMn_{1.6}Al_{0.4}$ [24] when X = Al. These $GdMn_2$-type phases are no longer visible on the XPD patterns of melt-spun samples (Fig. 1); they have turned into an amorphous state in every case. This is coherent with the fact that $GdMn_2$ can be easily obtained in amorphous state, as reported in [25].

Two broad halos centred around $2\theta = 32$ and 58° are clearly detected on the XPD patterns of melt-spun samples (Fig. 1); this behaviour is characteristic of the existence of an amorphous structure. XPD investigations also reveal appreciable peaks corresponding to the presence of crystalline phases in these samples. For instance, a very small peak attributable to α-Gd nanocrystallites [19] is visible near 28° on the XPD pattern of melt-spun $Gd_{60}Mn_{30}Ga_{10}$ (Fig. 1(a)). The existence of nanocrystallites in this sample was confirmed by TEM observation (Fig. 2(b)).

Similar analyses were performed on melt-spun $Gd_{60}Mn_{30}Al_{10}$ and $Gd_{60}Mn_{30}In_{10}$ samples (Fig. 1(b)). They revealed, respectively,

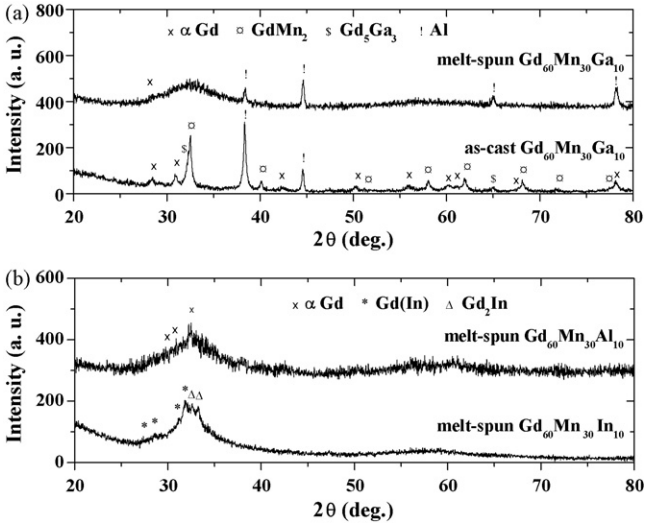

Fig. 1. XPD patterns of (a) as-cast and melt-spun $Gd_{60}Mn_{30}Ga_{10}$ samples and (b) melt-spun $Gd_{60}Mn_{30}Al_{10}$ and $Gd_{60}Mn_{30}In_{10}$ samples. Phases are identified by symbols as indicated on top of the figure. Peaks attributed to Al are due to the sample holder.

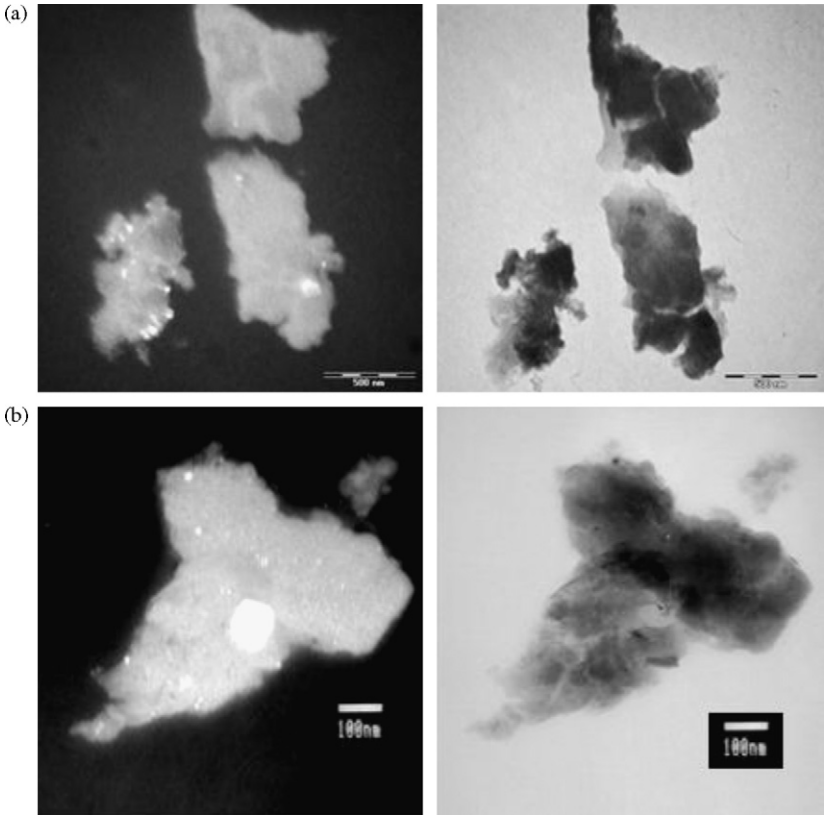

Fig. 2. TEM dark and white field micrographs of a fragment of melt-spun $Gd_{60}Mn_{30}In_{10}$ (a) and $Gd_{60}Mn_{30}Ga_{10}$ (b) ribbons showing nanocrystallites embedded into the amorphous matrix.

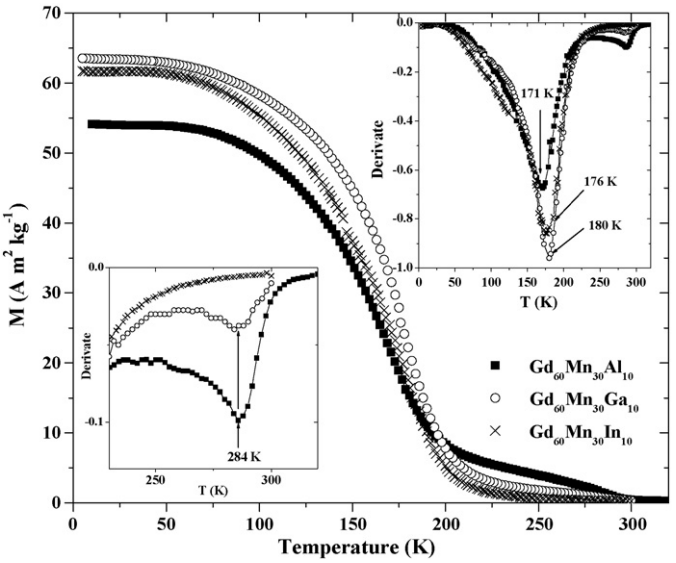

Fig. 3. Temperature dependence of the magnetization M, of melt-spun $Gd_{60}Mn_{30}Al_{10}$, $Gd_{60}Mn_{30}Ga_{10}$ and $Gd_{60}Mn_{30}In_{10}$, in a magnetic field of 0.05 T. The derivative curves $\partial(M)/\partial T$ on the full temperature domain are presented in inset of the top right part and a zoom of these derivative curves in the temperature range 230–320 K is shown in inset of the bottom left part.

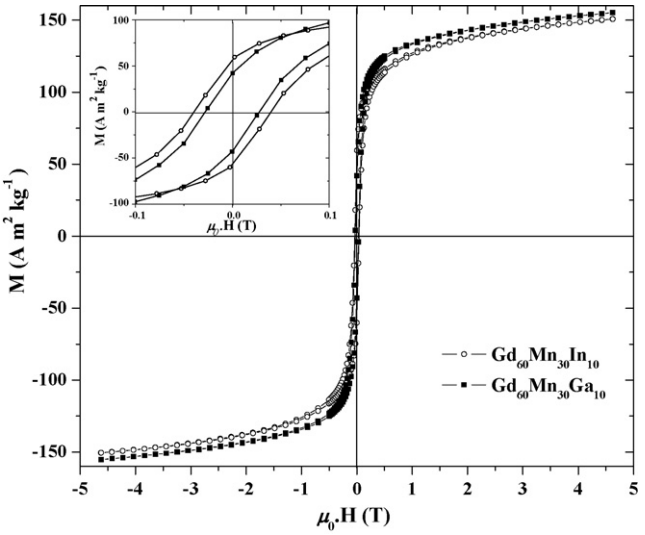

Fig. 4. Field dependence of the magnetization M, at 5 K, for melt-spun $Gd_{60}Mn_{30}In_{10}$ and $Gd_{60}Mn_{30}Ga_{10}$ samples. Inset is a zoom of this curve showing the coercive field and remanence of the samples.

the presence of α-Gd nanocrystallites in the first one; and Gd_2In binary indide [26] and Gd(In) solid solution [27] nanocrystallites in the latter. TEM micrographs obtained for melt-spun $Gd_{60}Mn_{30}In_{10}$ shown in Fig. 2(a) confirm the presence of small crystallites of size between 10 and 100 nm embedded in an amorphous matrix. Due to the very small degree of crystallization, TEM diffraction patterns corresponding to the micrographs shown in Fig. 2 could not lead to the identification of the crystallites for both melt-spun samples.

Fig. 3 shows the temperature dependence of the field cooled magnetization, *M versus T* curves for melt-spun samples, measured in an applied field of 0.05 T. The rather broad transitions at 171, 176 and 180 K (temperatures defined as the extreme on the derivative curve $\partial(M)/\partial T$ *versus T*), for $Gd_{60}Mn_{30}Al_{10}$, $Gd_{60}Mn_{30}In_{10}$ and $Gd_{60}Mn_{30}Ga_{10}$ respectively, visible on the three curves (inset of Fig. 3), are typical of a structurally disordered phase and can be attributed to the ferro(ferri)magnetic ordering of the amorphous matrix [20].

No magnetic transitions attributable to Gd_2In ($T_C \sim 200$ K) [28] or Gd(In) solid solution ($T_C = 248$ K) [27] nanocrystallites, detected by XPD in melt-spun $Gd_{60}Mn_{30}In_{10}$, appear on the *M versus T* plot (inset of Fig. 3). One possible explanation could be the presence of a magnetic dead layer at the surface of these nanocrystallites that would decrease their magnetization [29], and in this case reduces it to zero, considering the small amount of these crystallized particles. Another one could be the reduction of exchange-coupling between adjacent nanoparticles through the increasingly paramagnetic amorphous matrix when the sample's temperature is higher than the Curie temperature T_C of the amorphous matrix, as suggested by Hernando and Kulik [30]. The transition occurring at 284 K (inset of Fig. 3), for melt-spun $Gd_{60}Mn_{30}Ga_{10}$ and $Gd_{60}Mn_{30}Al_{10}$ samples, was identified as the ferromagnetic ordering of Gd atoms in α-Gd nanoparticles [7]. In this case, we assume that either the distance between crystallized particles is small enough for the exchange interactions to be possible between them or the exchange correlation length of these α-Gd particles is high, thus generating a magnetization measurable in an applied field of 0.05 T.

M versus $\mu_0 H$ curves obtained at 5 K, with magnetic field varying between −4.6 and 4.6 T, for melt-spun $Gd_{60}Mn_{30}In_{10}$ and $Gd_{60}Mn_{30}Ga_{10}$ samples show very small hysteresis (Fig. 4). Their coercive fields are rather low, respectively 0.039 and 0.028 T, as well as their remanence, respectively 56 and 42 A m^2 kg^{-1} (inset of Fig. 4). Both materials show a good cycling ability and their energy loss during a magnetization/demagnetization process is negligible (24.7 and 14.3 J kg^{-1} for $Gd_{60}Mn_{30}In_{10}$ and $Gd_{60}Mn_{30}Ga_{10}$ respectively).

Fig. 5 presents the field dependence of magnetization, *M versus* $\mu_0 H$ for melt-spun $Gd_{60}Mn_{30}In_{10}$ and $Gd_{60}Mn_{30}Ga_{10}$ samples, with a field increasing from 0 to 4.6 T and a temperature varying between 5 and 305 K, every 12.5 K and at 360 K. As these two materials are multiphased with crystallized phases difficult to quantify, it would induce an error to calculate the magnetic moment per unit formula or per mole of Gd, as it is usually done, to study the ordering of Gd in the amorphous phase only. One correct calculation is to compare the magnetization at saturation of $Gd_{60}Mn_{30}In_{10}$ and $Gd_{60}Mn_{30}Ga_{10}$ per mass of Gd to the maximal magnetization theoretically achievable with 1 kg of Gd at the ferromagnetic ordering saturation. In this study, the conditions of 5 K and 4.6 T are those in which the samples are closest to their saturation state (still, it is obvious that the *M versus* $\mu_0 H$ curves do not saturate). In these conditions, magnetization values expressed per mass of Gd for both samples are 195.5 and 191.0 A m^2 kg (Gd)$^{-1}$ for $Gd_{60}Mn_{30}In_{10}$ and $Gd_{60}Mn_{30}Ga_{10}$, respectively. This represents 79 and 77% of the magnetization reached with 1 kg of Gd (in saturated ferromagnetic order, calculated with the magnetic moment of 7 μ_B for the free Gd^{3+} ion). Even though saturation may not be reached at 4.6 T in these samples, these results suggest that a second magnetic sublattice orders antiferromagnetically towards that of Gd^{3+} ions in the amorphous matrix, decreasing the overall measured magnetization. As suggested by the results of Talik et al. [31] on $GdMn_2$, and Chevalier et al. [32] on GdMnAl, this could be due to an antiferromagnetic interaction between Gd and Mn sublattices, already observed in $GdMn_2$ and GdMnAl.

For an isothermal process, the magnetic entropy change ΔS_M can be calculated by integrating the Maxwell equation [33]:

$$\Delta S_M = \int_0^H \left(\frac{\partial M}{\partial T}\right)_H dH \quad (1)$$

In the case of magnetization measurements performed at small field and temperature increments, the following numerical approximation can be applied to calculate, for a given field change ΔH_m,

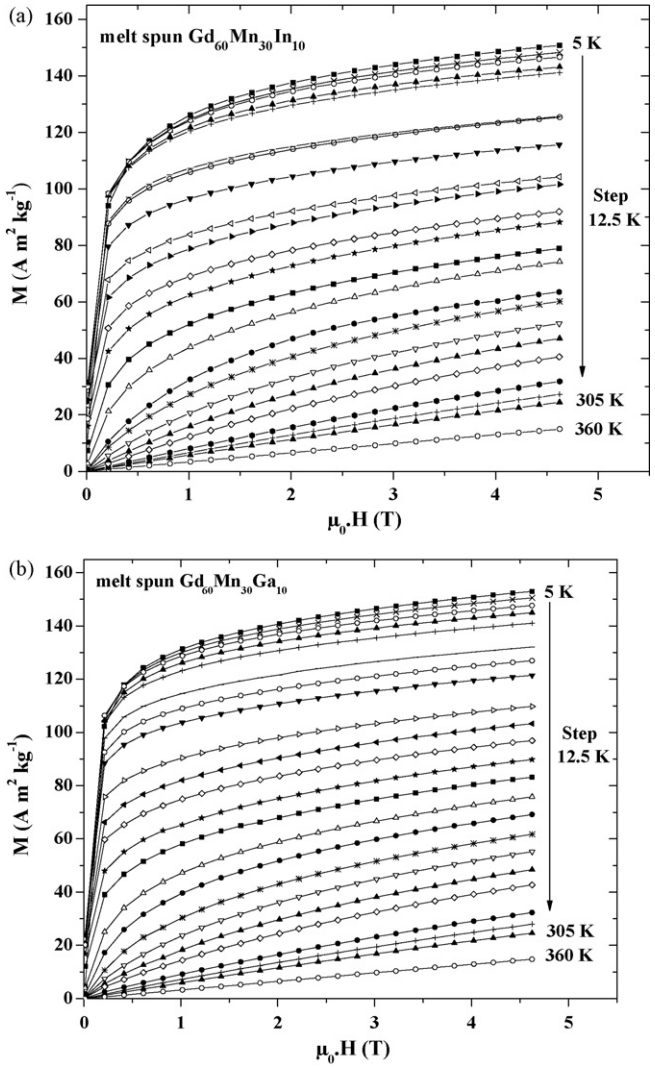

Fig. 5. Field dependence of the magnetization M, in the temperature range 5–305 K and at 360 K, for melt-spun $Gd_{60}Mn_{30}In_{10}$ (a) and $Gd_{60}Mn_{30}Ga_{10}$ (b) samples.

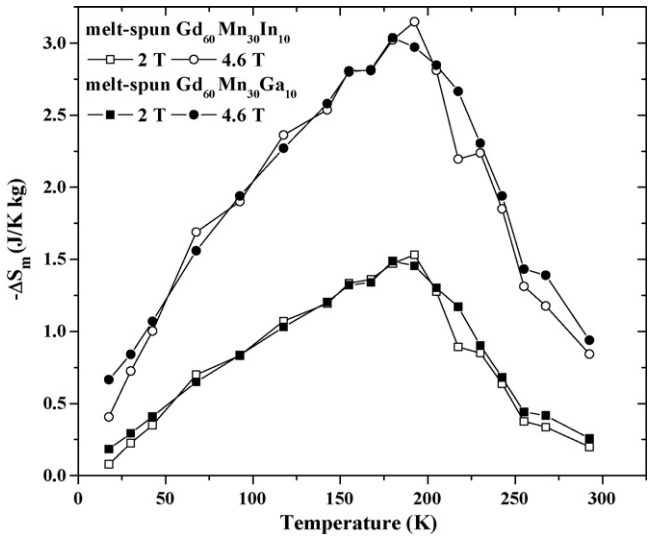

Fig. 6. Temperature dependence of the magnetic entropy change ΔS_M for both melt-spun $Gd_{60}Mn_{30}In_{10}$ and $Gd_{60}Mn_{30}Ga_{10}$ samples, in applied fields of 2 and 4.6 T.

the thermal dependence of ΔS_M: with T_i^{mean} defined as $T_i^{mean} = (T_{i+1} - T_i)/2$, $i \in [1, n-1]$ and $\Delta H_m = H_m - H_0$, Eq. (1) can be discretized as follows:

$$\Delta S_M\left(T_i^{mean}\right)_{\Delta H_m} = \sum_{j=1}^{m-1}\left[\left(\frac{M_{i+1,j} - M_{i,j}}{T_{i+1} - T_i}\right).(H_{j+1} - H_j)\right] \quad (2)$$

where $M_{i,j}$ and $M_{i+1,j}$ are the magnetization values measured at temperatures T_i and T_{i+1} in a field of H_j.

The ΔS_M temperature dependence was calculated (with Eq. (2)) for melt-spun $Gd_{60}Mn_{30}In_{10}$ and $Gd_{60}Mn_{30}Ga_{10}$ samples in applied fields of 2 and 4.6 T (Fig. 6). The peak values of ΔS_M are -1.53 and $-1.49\,J\,kg^{-1}\,K^{-1}$ at 2 T, and -3.15 and $-3.04\,J\,kg^{-1}\,K^{-1}$ at 4.6 T, for melt-spun $Gd_{60}Mn_{30}In_{10}$ and $Gd_{60}Mn_{30}Ga_{10}$ samples, respectively. These values are smaller than that of most refrigerant materials. The temperature width at half maximum value of ΔS_M is 157 K for both materials in a field change of 2 T, and 190 and 200 K at 4.6 T for melt-spun $Gd_{60}Mn_{30}In_{10}$ and $Gd_{60}Mn_{30}Ga_{10}$ samples, respectively. These values, on the contrary, are very high, even for amorphous alloys [34]. As mentioned in introduction, the refrigeration capacity (RC) is defined as the area below the ΔS_M *versus* T curve with the temperatures at half maximum of the peak as the integration limits [3]. When a material shows a hysteretic behaviour, it is necessary to subtract the hysteresis loss to get a more real RC value. But for the Gd-based metallic glasses studied here, the hysteresis loss is negligible (Fig. 4). At 4.6 T, the RC values are 451 (with a calculated hysteresis loss of 5.5% during a cycle) and $472\,J\,kg^{-1}$ (with a calculated hysteresis loss of 3.0% during a cycle) for melt-spun $Gd_{60}Mn_{30}In_{10}$ and $Gd_{60}Mn_{30}Ga_{10}$ samples, respectively.

The plots of ΔS_M^{peak} and RC values per applied magnetic field unit *versus* the Curie temperature (T_C), for several Gd-based metallic glasses from this work and literature are shown in Fig. 7. These two characteristic values were given per field unit only to get free from the different field change values used for the measurements (4.6 and 5 T). They are also compared to two Fe-based amorphous alloys with T_C near room temperature [35,36].

The global trend visible in Fig. 7(a) is a decrease of ΔS_M^{peak} values with the elevation of T_C, whatever the transition metal used for Gd-based samples. It is clear from this plot that the choice of Mn as transition element increases the T_C temperature of the material and reduces its ΔS_M^{peak} value. The possible antiferromagnetic coupling between Mn and Gd explaining this behaviour is being studied currently. This plot also shows that nanocomposite materials, reported with Co or Mn as transition elements, reach smaller ΔS_M^{peak} values than amorphous materials. In nanocomposite materials, a nonnegligible percentage of the total mass of Gd has crystallized and will not participate to the magnetization of the amorphous matrix. So for a same global composition, results of nanocomposite materials are lower than that of amorphous materials.

In Fig. 7(b), we can see that, in terms of RC values, materials with M = Mn or Fe compare well with the others. This is linked to the broadening of ΔS_M peak when the transition metal used is Mn or Fe.

The choice of the transition metal also appears to be determinant in the magnetic behaviour, especially for adjusting the T_C value. Indeed, the use of Co or Ni seems to limit T_C to low values and provides rather good ΔS_M^{peak} values, while using Fe or Mn favours higher T_C values and decreases ΔS_M^{peak}. The comparison with Fe-based ribbons, that display ferromagnetic transitions near room temperature, shows that $Gd_{60}Mn_{30}X_{10}$ materials reach slightly smaller ΔS_M peak values but still, higher RC values due to the observed widening of the ΔS_M *versus* T peak.

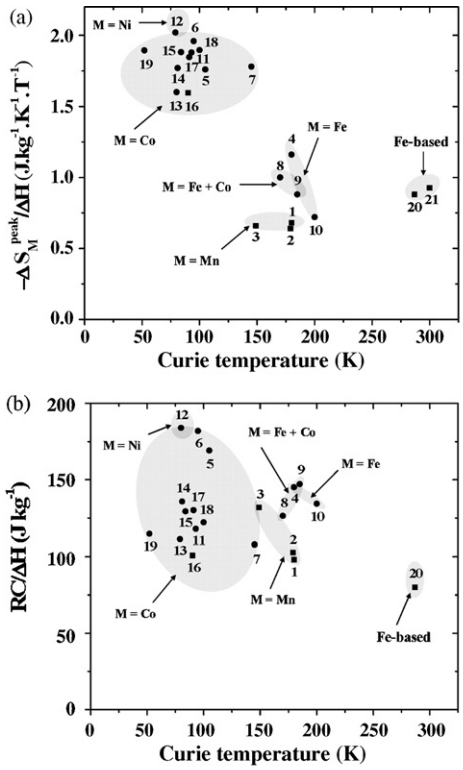

Compounds legend

1 - $Gd_{60}Mn_{30}In_{10}$ [this work]	8 - $Gd_{60}Fe_{10}Co_{20}Al_{10}$ [15]	15 - $Gd_{48}Al_{25}Co_{20}Zr_3Er_4$ [13]
2 - $Gd_{60}Mn_{30}Ga_{10}$ [this work]	9 - $Gd_{60}Fe_{20}Co_{10}Al_{10}$ [15]	16 - $Gd_{51}Al_{24}Co_{20}Nb_1B_4$ [13]
3 - $Gd_{60}Mn_{30}Al_{10}$ [7]	10 - $Gd_{60}Fe_{30}Al_{10}$ [15]	17 - $Gd_{51}Al_{24}Co_{20}Zr_4Nb_1$ [13]
4 - $Gd_{65}Fe_{20}Al_{15}$ [11]	11 - $Gd_{53}Al_{24}Co_{20}Zr_3$ [6]	18 - $Gd_{51}Al_{24}Co_{20}Nb_1Cr_4$ [13]
5 - $Gd_{55}Co_{20}Al_{25}$ [8]	12 - $Gd_{55}Ni_{25}Al_{20}$ [8]	19 - $Gd_{33}Er_{22}Al_{25}Co_{20}$ [6]
6 - $Gd_{52.5}Co_{16.5}Al_{31}$ [10]	13 - $Gd_{60}Co_{26}Al_{14}$ [14]	20 - $Fe_{88}Zr_7B_4Cu_1$ [35]
7 - $Gd_{60}Co_{30}Al_{10}$ [15]	14 - $Gd_{51}Al_{24}Co_{20}Ce_5$ [13]	21 – $Fe_{85}Zr_{10}B_5$ [36]

Fig. 7. Magnetic entropy change (a) and RC values (b) per field unit *versus* the Curie temperature of several fully amorphous (circles) and nanocomposite (squares) Gd-based and Fe-based metallic glasses. Envelops group series of materials with the same transition metal and Fe-based materials.

4. Conclusion

$Gd_{60}Mn_{30}In_{10}$ and $Gd_{60}Mn_{30}Ga_{10}$ nanocomposites have been prepared by single-roller melt-spinning. In their temperature operating range (around 175–180 K), melt-spun $Gd_{60}Mn_{30}In_{10}$ and $Gd_{60}Mn_{30}Ga_{10}$ samples exhibit refrigeration capacities of 451 and 472 J kg^{-1}, respectively, in a field change of 4.6 T. Such values are rather good, if we consider their low ΔS_M^{peak} values. This enhancement is clearly due to the widening of the temperature range over which the two magnetic transitions occur by first, having a very large transition due to the amorphous phase and by combining this transition to that of nanocrystallites.

Changing the X p-element between Al, Ga or In induced the formation of different nanocrystallites embedded in the amorphous matrix. Among them, only α-Gd displayed a magnetic transition (T_C = 284 K) in melt-spun $Gd_{60}Mn_{30}Al_{10}$ and $Gd_{60}Mn_{30}Ga_{10}$ samples. On the contrary, melt-spun $Gd_{60}Mn_{30}In_{10}$ sample displayed the amorphous matrix transition only probably because of the effect of a magnetic dead layer at the surface of crystallized nanoparticles of Gd(In) and Gd_2In.

An antiferromagnetic coupling between Gd and Mn atoms is strongly suspected in these melt-spun materials. It seems, then, very interesting to investigate the impact of the transition metal on the overall behaviour in such samples with different M by means of magnetization measurements under high magnetic fields up to 70 T to observe the saturation of these materials.

Acknowledgement

The authors are indebted to the Conseil Régional d'Aquitaine for financial support, especially C.M. for a Ph.D. grant.

References

[1] J. Glanz, Science 279 (1998) 2045.
[2] W.F. Giauque, J. Am. Chem. Soc. 49 (1927) 1864–1870.
[3] K.A. Gschneidner Jr., V.K. Pecharsky, A.O. Pecharsky, C.B. Zimm, Mater. Sci. Forum 69 (1999) 315–317.
[4] M. Foldeaki, R. Chahine, B.R. Gopal, T.K. Bose, X.Y. Liu, J.A. Barclay, J. Appl. Phys. 83 (1998) 2727–2773.
[5] L. Si, J. Ding, Y. Li, B. Yao, H. Tan, Appl. Phys. A: Mater. Sci. Process. 75 (2002) 535–539.
[6] Q. Luo, Q. Zhao, M.X. Pan, W.H. Wang, Appl. Phys. Lett. 89 (2006) 081914.
[7] S. Gorsse, B. Chevalier, G. Orveillon, Appl. Phys. Lett. 92 (2008) 122501.
[8] J. Du, Q. Zheng, Y.B. Li, Q. Zhang, D. Li, Z.D. Zhang, J. Appl. Phys. 103 (2008) 023918.
[9] J. Du, Q. Zheng, E. Bruck, K.H.J. Buschow, W.B. Cui, W.J. Feng, Z.D. Zhang, J. Magn. Magn. Mater. 321 (2009) 413–417.
[10] H. Fu, M.S. Guo, H.J. Yu, X.T. Zu, J. Magn. Magn. Mater. 321 (2009) 3342–3345.
[11] Q.Y. Dong, B.G. Shen, J. Chen, J. Shen, F. Wang, H.W. Zhang, J.R. Sun, J. Appl. Phys. 105 (2009) 053908.
[12] Q. Luo, D.Q. Zhao, M.X. Pan, W.H. Wang, Appl. Phys. Lett. 90 (2007) 211903.

[13] Q. Luo, W.H. Wang, J. Alloys Compd. 495 (2010) 209–216.
[14] H. Fu, X.Y. Zhang, H.J. Yu, B.H. Teng, X.T. Zu, Solid State Commun. 145 (2008) 15–17.
[15] B. Schwarz, B. Podmilsak, N. Mattern, J. Eckert, J. Magn. Magn. Mater. 322 (2010) 2298–2303.
[16] M.F. Ashby, A.L. Greer, Scripta Mater. 54 (2006) 321–326.
[17] D. Miracle, Nat. Mater. 3 (2004) 697–702.
[18] G. Orveillon, O.N. Senkov, J.L. Soubeyroux, B. Chevalier, S. Gorsse, Adv. Eng. Mater. 9 (2007) 483–486.
[19] F. Spedding, J. Hanak, A. Daane, J. Less-Common Met. 3 (1961) 110–124.
[20] X.Y. Liu, J.A. Barclay, R.B. Gopal, M. Foldeaki, R. Chahine, T.K. Bose, P.J. Schurer, J.L. LaCombe, J. Appl. Phys. 79 (1996) 1630–1641.
[21] J. Zhao, J.D. Corbett, J. Alloys Compd. 210 (1994) 1–7.
[22] A.V. Morozkin, D. Yu, A.V. Gribanov, J.M. Barakatova, J. Alloys Compd. 256 (1997) 175–191.
[23] S. DeNegri, D. Kaczorowski, A. Grytsiv, A. Alleno, M. Giovannini, R. Gorzelniak, P. Rogl, C. Godart, A. Saccone, R. Ferro, J. Alloys Compd. 365 (2004) 58–67.
[24] A. Slebarski, A. Chelkowski, J. Less-Common Met. 57 (1978) 125–131.
[25] B. Chevalier, J.L. Bobet, M. Nakhl, J. Etourneau, J. Alloys Compd. 320 (2001) 33–39.
[26] A. Palenzona, J. Less-Common Met. 16 (1968) 379–384.
[27] W.J. Ren, D. Li, W. Liu, J. Li, Z.D. Zhang, J. Appl. Phys. 103 (2008), B32307.
[28] J. Szade, J. Magn. Magn. Mater. 170 (1997) 228–234.
[29] A. Tamion, C. Raufast, M. Hillenkamp, E. Bonet, J. Jouanguy, B. Canut, E. Bernstein, O. Boisron, W. Wernsdorfer, V. Dupuis, Phys. Rev. B 81 (2010) 144403.
[30] A. Hernando, T. Kulik, Phys. Rev. B 49 (1993) 7064–7067.
[31] E. Talik, M. Neumann, T. Mydlarz, J. Kusz, H. Böhm, A. Winiarski, A. Gilewski, J. Phys.: Condens. Matter 10 (1998) 581–592.
[32] B. Chevalier, J.L. Bobet, J. Etourneau, J. Alloys Compd. 339 (2002) 35–39.
[33] A.H. Morrish:, The Physical Principles of Magnetism, John Wiley & Sons, New York, 1964.
[34] Q. Luo, W. Wang, J. Non-Cryst. Solids 355 (2009) 759–775.
[35] R. Caballero-Flores, V. Franco, A. Conde, K.E. Knipling, M.A. Willard, Appl. Phys. Lett. 96 (2010) 182506.
[36] Y. Wang, X. Bi, Appl. Phys. Lett. 95 (2009) 262501.